Numerical Analysis of Two Phase Cross-Flow Heat Exchanger for High Power Density Equipment in Data Centers under Dynamic Conditions

Carol Caceres[+], Alfonso Ortega[*], Aaron Wemhoff[**], Gerard F. Jones[++]
Villanova University
Villanova, PA, USA, 19085
Email: [+]acacere4@villanova.edu
[*]alfonso.ortega@villanova.edu
[**]aaron.wemhoff@villanova.edu
[++]gerard.jones@villanova.edu

ABSTRACT

Computational demand in the IT sector has increased dramatically and so rack level power densities from 10 to 50 kW/rack are increasingly common. Expanding the capabilities of the IT equipment requires thermal management systems able to handle time dependent thermal loads. Emerging system designs will almost certainly have to utilize close-coupled cooling subsystems to augment or replace traditional centralized perimeter air handlers. Distributed cooling technologies such as close-coupled rear-door heat exchangers, overhead heat exchangers, and in-row cooler heat exchangers have been developed to meet these high demands. To increase the thermal performance of the cross-flow heat exchangers, two phase flow is used with low-boiling-point refrigerants such as R134a, R407c, and R410a. In this study, a physics-based numerical model for cross-flow heat exchanger is developed in order to understand dynamic behavior. A system of partial differential equations for mass, momentum, and energy conservation has been solved using the finite difference method and implemented in MATLAB. Thermodynamic properties are obtained from COOLPROP. The dynamic model of cross-flow heat exchangers may be used to develop improved control strategies and increase energy efficiencies to meet the ever-increasing cooling demands of data centers.

KEY WORDS: Cross-Flow Heat Exchangers, Data Center, Two Phase

NOMENCLATURE

A	Area, m^2
c	Specific heat, J/kg K
D	Diameter, m
E	Enhancement factor
f	Friction factor
Fr	Froude number
F_p	Fin pitch, m
G	Mass flux, kg/m^{2}s
h	Enthalpy, J/kg
$\tilde{h}$	Average enthalpy, J/kg
H	Heat transfer coefficient, W/m^{2}K
j	Colburn factor
k	Conductivity, W/m K
$\dot{m}$	Mass flow rate, kg/s
M	Mass, kg
M	Molecular weight, gr/mol
p	Pressure, kPa
Pr	Prandtl number
P_l	Longitudinal tube pitch, m
P_d	Waffle height, m
q''	Heat flux, W/m^2
Re	Reynolds number
S	Slip-ratio
$\breve{S}$	Suppression factor
T	Temperature, K
u	Velocity, m/s
X_f	Projected wavy length, m
x	Quality

Greek symbols

α	Void fraction
γ	Advection momentum multiplier
δ	Thickness, m
ε	Convergence tolerance
η	Efficiency
ρ	Density, kg/m^3
$\tilde{\rho}$	Average Density, kg/m^3
ϕ	Two phase friction multiplier

Subscripts

a	Air
c	Collar
$c-a$	Cross sectional area
cr	Critical
f	Fin
go	Gas only
l	Saturated liquid
lo	Liquid only
r	Refrigerant
$t-p$	Two phase
v	Saturated gas
w	Wall
w & l	Wall and liquid contact
w & v	Wall and gas contact

INTRODUCTION

Data center power density is continuously increasing. High power density data centers have had to migrate to new technologies such as close-coupled hybrid air-liquid cooling systems. Specifically, rear door heat exchangers, overhead heat exchangers, in-row coolers and rack enclosures are used for high density racks [1].

Figure 1 highlights some differences between classical centralized and close-coupled cooling techniques. For instance, classical data centers (Fig. 1a) deliver cooling through a raised floor. Controlling the amount of cold air to the servers with centralized cooling is not simple and does not reduce the presence of hot spots. On the other hand, a close-coupled system (Fig. 1b, Fig. 1c, and Fig. 1d) is proximate to the servers, offering opportunities of controlling the amount of local cooling delivered. Rear door, in-row, and overhead units are equipped with dedicated fans controlled by variable frequency drives that are controlled to deliver flow as needed by the load. Thus, close coupled cooling technologies increase energy efficiency by providing cold air to the servers according to demand.

a) Centralized cooling system b) Rear door

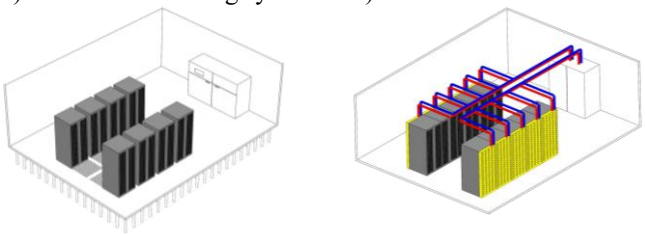

c) In-row d) Overhead

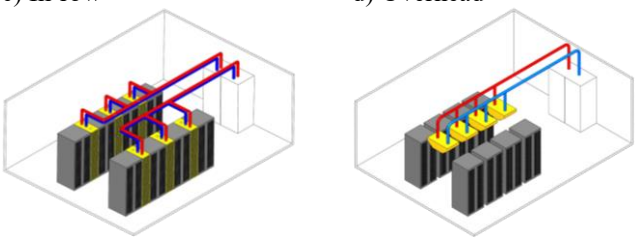

Fig. 1. a) Classical centralized cooling system. b), c), and d), Close coupled hybrid air-liquid cooling system

The load on the servers is variable with time, affecting the reaction of the hybrid cooling system. Hence, the dynamic behavior of these cooling technologies must be understood in order to develop effective control strategies.

Del Valle et al. [2-5] and Gao et al. [6, 7] studied the transient response of a cross flow heat exchanger, which is the heart of close-coupled system. These studies were focused on heat exchange using chilled water for data center applications. The authors developed transient models for a single-phase cross-flow heat exchanger. The current paper investigates the transient behavior of refrigerant based evaporators. The capacity and performance gains in two phase heat exchangers makes them an attractive option as thermal load continues increase.

The most common transient studies on cross-flow heat exchangers are related to HVAC systems. In these systems, the refrigerant condition at the outlet of the evaporator is saturated vapor or superheat. In the modeling of dynamic HVAC systems, the evaporator and condenser use the moving boundary model [8-11] assuming an average void fraction. This assumption simplifies the transient modeling of heat exchangers since several components such as compressors and expansion valves must be considered in the simulation. The refrigerant outlet condition in close-coupled systems is two phase. Vapor quality at the outlet of the heat exchanger ensures that the heat exchange is maximized due to the high heat transfer coefficient in two phase flow. The objective of this investigation is to develop an accurate computational model for a dynamic refrigerant based evaporator. In this work, the prediction of the thermodynamic quality distribution is crucial. Slip-ratio effects are also considered in the proposed model, affecting the quality distribution and the quality at the outlet of the heat exchanger.

HEAT EXCHANGER CHARACTERISITICS

In order to generate a model for cross-flow heat exchangers, important physical characteristics of the device are needed. These characteristics are length dimensions, fin geometry, materials of the heat exchanger itself, and operating conditions. According the parameters mentioned, an available heat exchanger was chosen for typical geometry measurements and materials. The thermal mass and heat capacitance were calculated since they are needed in the energy equations. The cross-flow heat exchanger and its main characteristics are shown in Fig. 2 and Table 1. The heat exchanger is the same as used by Del Valle el al. [2-5]

Fig. 2. Cross-flow heat exchanger.

Table 1. Heat Exchanger Geometry.

Pipe ID	5/8 in
Pipe Material	Copper
Fin Type	Wavy
Fins Material	Aluminum
Fins per inch	10
Dimensions	12x12x5 inches

CROSS-FLOW HEAT EXCHANGER ANALYSIS

The heat exchanger transfers heat between two working fluids, air and refrigerant. The materials of construction and the configuration of flow passages greatly affect heat exchanger performance. Figure 3 shows the working fluid and as well as pipe and fins that are involved in heat transfer processes.

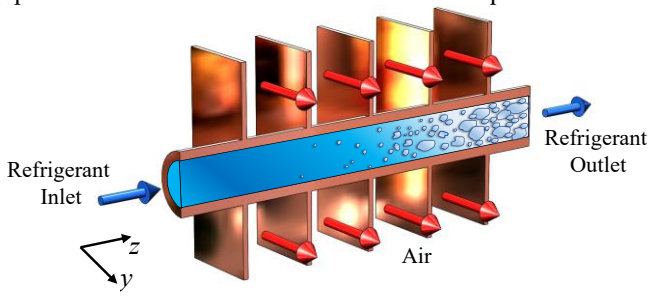

Fig. 3. Cross-Flow Heat Exchanger Scheme.

Air Energy Equation

A transient energy balance is obtained for the air side, where the air flows in y direction as shown as in Fig. 3. The equation neglects the axial conduction effects.

$$\Delta M_a c_a \frac{\partial T_a}{\partial t} + \dot{m}_a c_a \Delta y \frac{\partial T_a}{\partial y} + \Delta A_a \eta_f H_a (T_a - T_w) = 0 \quad (1)$$

A heat transfer coefficient is needed in Eq. (1). A suitable correlation is used to obtain the air side heat transfer coefficient. Based on extensive experiments, Wang [12] found correlations based on geometrical parameters and air conditions. The numerical model includes the following equations to calculate the heat transfer coefficient, H_a.

$$j = 1.79097 \mathrm{Re}_{Dc}^{J1} \left(\frac{P_l}{\delta_f}\right)^{-0.456} N^{-0.27} \left(\frac{F_p}{D_c}\right)^{-1.343} \left(\frac{P_d}{X_f}\right)^{0.317} \quad (2)$$

where $J1$ in the Colburn factor is defined as,

$$J1 = -0.1707 - 1.374 \left(\frac{P_l}{\delta_f}\right)^{-0.493} \left(\frac{F_p}{D_c}\right)^{-0.886} N^{-0.143} \left(\frac{P_d}{X_f}\right)^{-0.0296} \quad (3)$$

and,

$$H_a = \frac{j \rho_a u_a c_a}{\mathrm{Pr}_a^{2/3}} \quad (4)$$

Wall Energy Equation

The wall energy balance is performed considering the fins and the pipe together as the wall of the heat exchanger. The energy equation follows assumptions and analysis found in Mishra et al. [13-15], Syed and Idem [16], Del Valle et al. [2-5] and Gao [6, 7]. Hence, the transient energy balance equation for the heat exchanger wall becomes

$$\Delta M_w c_w \frac{\partial T_w}{\partial t} + \Delta A_a \eta_f H_a (T_w - T_a) + \Delta A_r H_r (T_w - T_r) = 0 \quad (5)$$

Note that Eq. (5) contains the refrigerant-side heat transfer with its associated heat transfer coefficient, H_r. The expression used to obtain the heat transfer coefficient for the refrigerant will be covered in the next section.

Refrigerant Equations

Studies have been performed for cross-flow heat exchangers in HVAC equipment, achieving superheat or saturated vapor at the outlet of the exchanger. In close-coupled systems, the refrigerant at outlet of the heat exchanger is a two phase mixture. Several insights and the analysis in this section have been extracted from Jia et al. [17-19] and Kapadia et al. [20]. The governing equations for the refrigerant side considers a one dimensional two phase flow.

The continuity equation is,

$$\frac{\partial \tilde{\rho}_r}{\partial t} + \frac{\partial \tilde{\rho}_r u}{\partial z} = 0 \quad (6)$$

where the average density is defined in terms of saturated densities and the void fraction α:

$$\tilde{\rho}_r = \alpha \rho_v + (1 - \alpha) \rho_l \quad (7)$$

The void fraction is an important parameter that characterizes the portion of gas and liquid. The void fraction is defined by

$$\alpha = \frac{1}{1 + S \frac{\rho_v}{\rho_l} \frac{1-x}{x}} \quad (8)$$

$$S = \frac{u_v}{u_l} \quad (9)$$

where S is the slip-ratio, or the ratio between the vapor and liquid velocity in the two phase.

The momentum equation is included in order to predict the local pressure which affects the thermodynamics properties in the flow:

$$\frac{\partial}{\partial t}(\tilde{\rho} u) + \frac{\partial}{\partial z}(\gamma \tilde{\rho} u^2) = -\frac{\partial p}{\partial z} - f_z \quad (10)$$

The term γ in Eq. (10) accounts for the acceleration of the vapor compared to the liquid:

$$\gamma = \frac{(x - Sx - 1)(Sx - x - S)}{S} \quad (11)$$

The source term f_z in Eq. (10) corresponds to the frictional forces between the vapor and the wall, and the liquid and the wall:

$$f_z = f_{w\&l} + f_{w\&v} \quad (12)$$

Equation (12) is evaluated using the correlation proposed by Müller and Heck [21]. In order to obtain the frictional pressure gradient the following expression is calculated;

$$f_z = \left(\frac{\partial p}{\partial z}\right)_{t\text{-}p} = \phi_{lo}^2 \left(\frac{\partial p}{\partial z}\right)_{lo} \tag{13}$$

where, the pressure gradient in two phase flow due to friction forces depends on a frictional multiplier and the gradient pressure when the fluid flow is considered liquid. The multiplier according Müller and Heck [21] is

$$\phi_{lo}^2 = Y^2 x^3 + (1-x)^{1/3}\left[1 + 2x\left(Y^2 - 1\right)\right] \tag{14}$$

where

$$Y^2 = \frac{(\Delta p/\Delta L)_{go}}{(\Delta p/\Delta L)_{lo}} \tag{15}$$

$$\left(\frac{\Delta p}{\Delta L}\right)_{lo} = \frac{G^2}{2D\rho_l} \mathrm{f}_{lo} \tag{16}$$

and

$$\left(\frac{\Delta p}{\Delta L}\right)_{go} = \frac{G^2}{2D\rho_v} \mathrm{f}_{go} \tag{17}$$

Friction factors for Eqs. (16) and (17) are calculated with the Fang and Zhou [22] expression, where a smooth pipe is assumed.

$$\mathrm{f} = 0.25\left[\log\left(\frac{150.39}{\mathrm{Re}^{0.98865}} - \frac{152.66}{\mathrm{Re}}\right)\right]^{-2} \tag{18}$$

A refrigerant two phase velocity is defined as

$$u = \frac{G}{\tilde{\rho}_r} \tag{19}$$

Equation (19) will be used in the homogenous and non-homogeneous analysis.

Finally, to complete the set of equations the energy equation in the refrigerant is obtained as

$$\frac{\partial \tilde{h}_r}{\partial t} + \frac{\partial \tilde{\rho}_r h_r u}{\partial z} + \frac{\pi D}{A_{c-a}} H_r (T_r - T_w) = 0 \tag{20}$$

Two types of enthalpy are in the refrigerant energy equation, the average enthalpy Eq. (21) and the thermodynamic enthalpy Eq. (22).

$$\tilde{h}_r = \alpha \rho_v h_v + (1-\alpha)\rho_l h_l \tag{21}$$

$$h_r = x h_v + (1-x) h_l \tag{22}$$

As in Eq. (5), Eq. (20) contains the heat transfer coefficient, H_r. A well-known correlation to evaluate the heat transfer coefficient for two phase flow is given by Liu and Winterton [23].

$$H_r = \{(\mathrm{E}\cdot \mathrm{E}_2 \cdot H_{lo})^2 + (\breve{S}\cdot \breve{S}_2 \cdot H_{pool})^2\}^{1/2} \tag{23}$$

A horizontal pipe is assumed and $Fr_{lo} > 0.05$, therefore E_2 and S_2 are equal to 1. Therefore,

$$H_r = \{(\mathrm{E}\cdot H_{lo})^2 + (\breve{S}\cdot H_{pool})^2\}^{1/2} \tag{24}$$

where the enhancement factor E is,

$$\mathrm{E} = \left(1 + x\cdot Pr_l\left(\frac{\rho_l}{\rho_v} - 1\right)\right)^{0.35} \tag{25}$$

and the suppression factor S is,

$$\breve{S} = \frac{1}{1 + 0.055\mathrm{E}^{0.1}\mathrm{Re}_l^{0.16}} \tag{26}$$

In the first term on the right hand side in Eq. (24), a heat transfer coefficient correlation is needed. The Dittus-Boelter relation was used and evaluated in terms of saturated liquid properties:

$$H_{lo} = 0.023\left(\frac{k_l}{d}\right)\mathrm{Re}_l^{0.8}\,\mathrm{Pr}_l^{0.4} \tag{27}$$

The pool boiling heat transfer coefficient is calculated with the expression proposed by Cooper [24].

$$H_{pool} = 55\left(\frac{p}{p_{cr}}\right)\left(-\log\left(\frac{p}{p_{cr}}\right)\right)^{-0.55}\mathrm{M}^{-0.5}(q'')^{2/3} \tag{28}$$

Following the analysis presented by Wallis [25], the continuity (6) and energy equation (20) are combined to get,

$$\frac{\partial \tilde{h}_r}{\partial t} - h_r \frac{\partial \tilde{\rho}_r}{\partial t} + \tilde{\rho}_r u \frac{\partial h_r}{\partial z} + \frac{\pi D}{A_{c-a}} H_r (T_r - T_w) = 0 \tag{29}$$

Equation (29) is analyzed in the two next subsections for a homogenous and then a non-homogeneous two phase flow.

Homogeneous Analysis Refrigerant Equations

In a homogeneous analysis it is assumed that the slip-ratio is equal to one. In other words, the vapor and liquid velocity are the same.

Substituting S=1 into the equations (7), (8), (19), (21), (22), into Eq. (29) leads to,

$$\frac{\rho_v \rho_l h_{fg}}{\rho_v + x(\rho_l - \rho_v)} \frac{\partial x}{\partial t} + G h_{fg} \frac{\partial x}{\partial z} + \frac{\pi D}{A_{c-a}} H_r (T_r - T_w) = 0 \tag{30}$$

Equation (30) allows us to obtain the quality distribution. The solution for this equation will be explained in the numerical section method. Additionally, in the momentum equation, the factor γ for a homogeneous flow is also equal to 1.

Refrigerant Equations for Non-Homogeneous Flow

For non-homogeneous flow,

$$S \neq 1,\ S = \text{function of } (x),\ x = \text{function of } (t, z) \tag{31}$$

The steps used to derive Eq. (30) are also used here, except that the slip-ratio now is a function of vapor quality, which is a function of time and position. The result is:

$$\frac{\rho_l h_{fg}\left(\left(\frac{\rho_l}{\rho_v}-1\right)x+1\right)\left(S+x(x-1)\frac{\mathrm{d}S}{\mathrm{d}x}\right)}{\left(-(1-x)S-\frac{\rho_l}{\rho_v}x\right)^2}\frac{\partial x}{\partial t}+ \qquad (32)$$
$$Gh_{fg}\frac{\partial x}{\partial z}+\frac{\pi D}{A_{c-a}}H_r(T_r-T_w)=0$$

Equation (32) depends on the slip-ratio which is quality dependent. Therefore, Eq. (32) can be expressed in terms of vapor quality. Ten models for slip-ratio were evaluated [25-34]. Figure 4 shows the resultant variation of slip-ratio with quality.

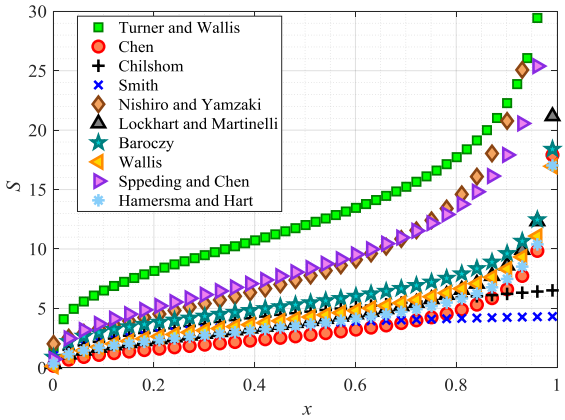

Fig. 4. Slip-ratio variation with vapor quality.

The upper and lower bound can be selected as shown by Awad and Muzychka [35]. The slip-ratio given by Turner and Wallis [28] is used as the upper bound:

$$S_{\text{Turner \& Wallis}}=\left(\frac{x}{1-x}\right)^{0.28}\left(\frac{\rho_l}{\rho_v}\right)^{0.6}\left(\frac{\mu_l}{\mu_v}\right)^{0.08} \qquad (33)$$

As seen, in Fig. 4 the lower limit is discernible until the point where the vapor quality is about 70%. The Chen [33] correlation is selected as the lower bound:

$$S_{\text{Chen}}=0.18\left(\frac{x}{1-x}\right)^{0.4}\left(\frac{\rho_l}{\rho_v}\right)^{0.67}\left(\frac{\mu_l}{\mu_v}\right)^{0.07} \qquad (34)$$

Introducing Eqs. (33) and (34) into Eq. (32) will result in an expression only in terms of vapor quality. The quality is the most important parameter that drives correlations as well as the fundamental equations.

Applying the relation by Turner and Wallis (Eq. (33)), into Eq. (32) yields

$$\frac{\rho_l h_{fg}\left(\left(\frac{\rho_l}{\rho_v}-1\right)x+1\right)\left(0.72\left(\frac{x}{1-x}\right)^{0.28}\left(\frac{\rho_l}{\rho_v}\right)^{0.6}\left(\frac{\mu_l}{\mu_v}\right)^{0.08}\right)}{\left(-x^{0.28}(1-x)^{0.72}\left(\frac{\rho_l}{\rho_v}\right)^{0.6}\left(\frac{\mu_l}{\mu_v}\right)^{0.08}-\frac{\rho_l}{\rho_v}x\right)^2}\frac{\partial x}{\partial t}+ \qquad (35)$$
$$Gh_{fg}\frac{\partial x}{\partial z}+\frac{\pi D}{A_{c-a}}H_r(T_r-T_w)=0$$

Combining Eqs. (34) and (32) results in the expression

$$\frac{\rho_l h_{fg}\left(\left(\frac{\rho_l}{\rho_v}-1\right)x+1\right)\left(0.108\left(\frac{x}{1-x}\right)^{0.4}\left(\frac{\rho_l}{\rho_v}\right)^{0.67}\left(\frac{\mu_l}{\mu_v}\right)^{0.07}\right)}{\left(-0.18x^{0.4}(1-x)^{0.6}\left(\frac{\rho_l}{\rho_v}\right)^{0.67}\left(\frac{\mu_l}{\mu_v}\right)^{0.07}-\frac{\rho_l}{\rho_v}x\right)^2}\frac{\partial x}{\partial t}+ \qquad (36)$$
$$Gh_{fg}\frac{\partial x}{\partial z}+\frac{\pi D}{A_{c-a}}H_r(T_r-T_w)=0$$

The slip-ratio equations (33) and (34) must also be introduced in Eq. (11) as well as the momentum Eq. (10).

NUMERICAL SOLUTION

The finite difference solution technique was used to solve the system of partial differential equations of Eqs. (1), (5), (10), (30), and (35) or (36). The wall equation (5) is discretized explicitly in time. The air equation (1) is discretized using backward differencing in space and backward differencing in time. Equations (10), (30), (35) and (36) are discretized in a similar way and described in the Appendix.

Equations (30), (35), and (36) are first solved to obtain quality. These are non-linear equations, therefore the equations must be solved iteratively. However, these equations have an embedded heat transfer coefficient, H_r which also is a quality-dependent parameter. In Cooper's Eq. (28) the heat transfer coefficient is embedded. Inserting Eq. (37) into Eq. (28) gives an implicit form of Eq. (23). Hence, iteratively the heat transfer coefficient is obtained using

$$q''_w=H_r(T_w-T_r) \qquad (37)$$

Equation (10) is used to calculate the local pressure. The results provide the local saturated properties. The flow chart of Fig. 5 shows the procedure to solve the system of equations.

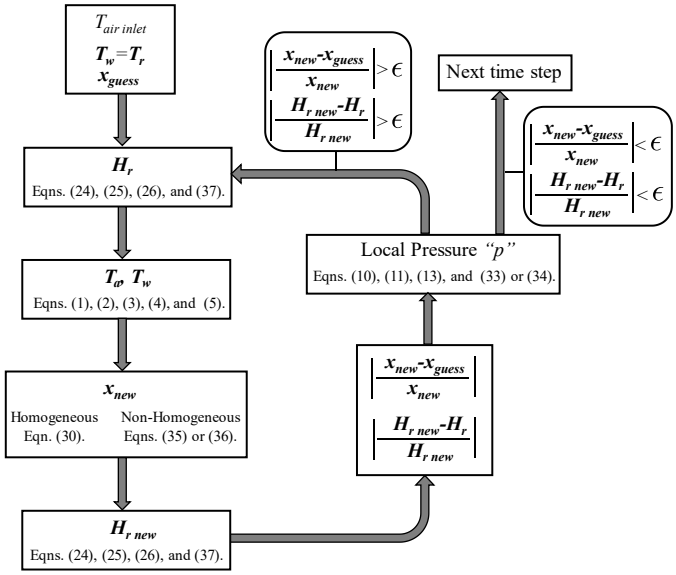

Fig. 5. Flow chart for numerical solution.

The perturbation of the air inlet temperature is the driving mechanism that generates changes over time in the heat exchanger. A ramp temperature simulating a jump in the air

temperature leaving the servers is used as the time dependent perturbation. Figure 6 shows the assumed inlet air temperature to the heat exchanger. Note that the air temperature is higher than the inlet refrigerant temperature so that the heat exchanger will behave as an evaporator. The air velocity used is 3.65 m/s. The mass flux of refrigerant is 410 kg/m^{2}s, and saturated conditions are considered at the inlet of the heat exchanger with a refrigerant temperature of 294K. These parameters were selected based on typical data center specifications. The refrigerant chosen is R134a. Refrigerants properties were obtained with COOLPROP [36] and connected to the calculations in MATLAB.

The heat exchanger thermal capacitance is 1348 J/K and the core mass is 1.81 kg based on the cross-flow heat exchanger shown in Fig. 2.

Under-relaxation was used in the iterative procedure. The relaxation parameter factor is taken as 0.5. Spatial discretization was studied, showing that between 80 to 100 nodes for the refrigerant gives mesh-independent results. The same number of nodes were used in the air flow direction. A small time step of 0.1 s was chosen to accurately track the solution. Typical run times were about 1-2 minutes.

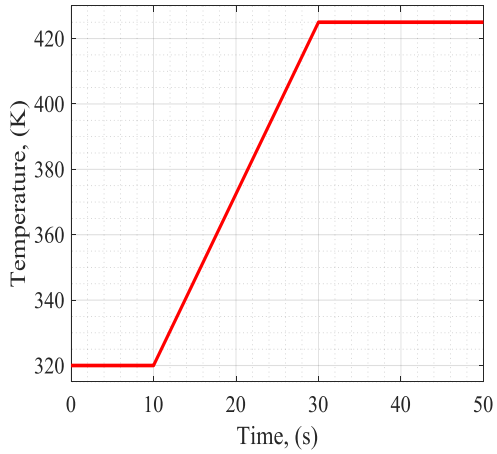

Fig. 6. Air temperature perturbation boundary condition.

RESULTS

Homogenous Flow Results

The inlet temperature of the refrigerant is less than the air temperature. Therefore, the refrigerant is heated by the air and will undergo evaporation. In doing so the quality will increase in the direction of the refrigerant flow and over time. Figure 7 shows quality as function of the total length of the refrigerant flow in the heat exchanger tube.

The HTC (heat transfer coefficient**)** shows the same trends of Fig. 7, with an increase in HTC values with distance in the direction of refrigerant flow and over time. Note that the magnitudes of HTC are much larger than one would normally expect from single phase flow of a liquid.

The wall temperature is shown in Fig 9. Wall temperature decreases over length as result of increasing HTC over length as seen in Fig. 8. Recall that the refrigerant temperature remains constant during the phase change. The wall temperature increases with time because of the assumed increase in air temperature of Fig. 7.

From Fig. 10, note that the pressure changes are generally small, but the local pressure affects the thermodynamic properties and thus the entire solution of the problem. Overall, the heat exchanger experiences a maximum pressure drop of about 4 kPa. Therefore, the influence of thermodynamic property variation due to pressure drop is minor.

The air outlet temperature is obtained and shown in Fig. 11. The air-side response is essential since the air leaving the heat exchanger will provide cooling to servers. Therefore, accurate predictions of air outlet temperature subject to variable cooling loads is crucial in a close-coupled system.

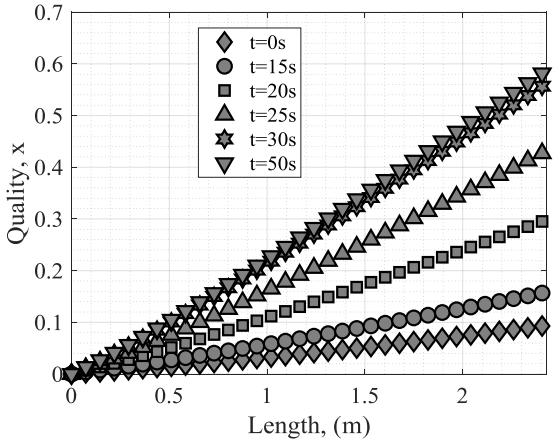

Fig. 7. Dynamic quality distribution. Homogeneous flow approach.

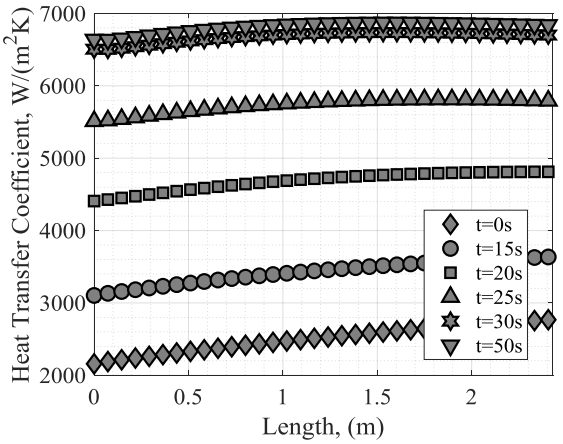

Fig. 8. Local heat transfer coefficient. Homogeneous flow approach.

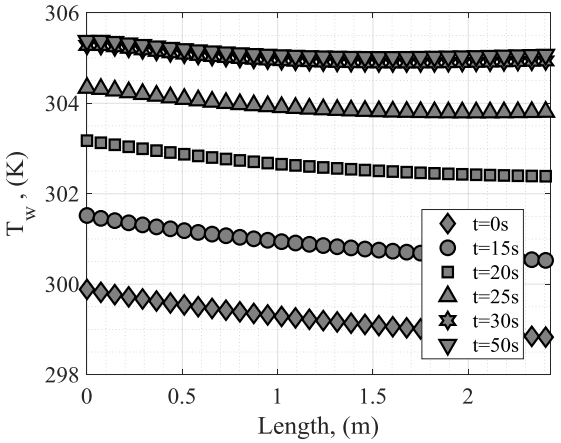

Fig. 9. Wall temperature. Homogeneous flow approach.

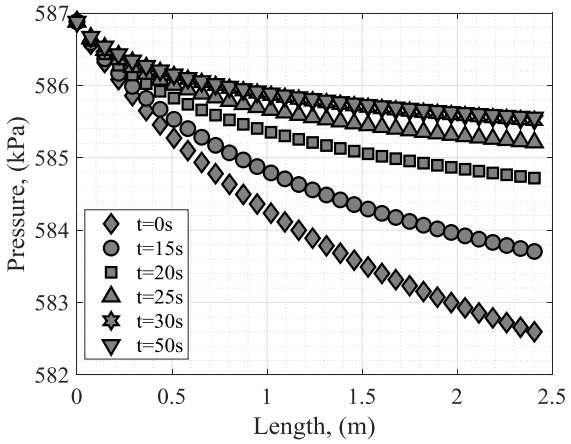

Fig. 10. Local pressure. Homogeneous flow approach.

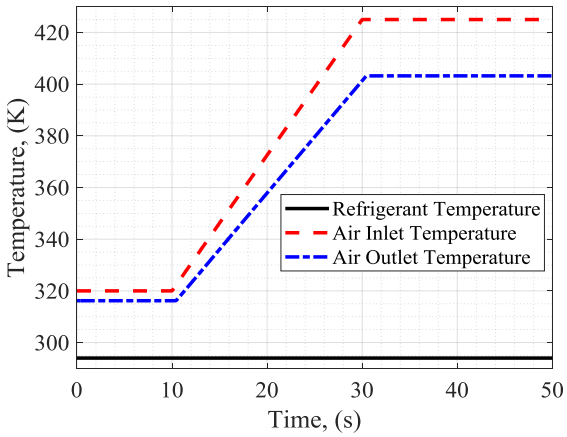

Fig. 11. Outlet air temperature response to perturbed air inlet temperature. Homogeneous flow approach.

Non-Homogenous Flow Approach Results

Adding slip-ratio effects alters the acceleration of the vapor relative to the liquid velocity.

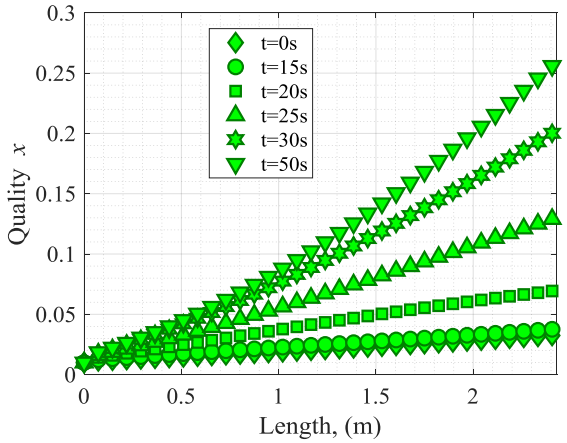

Figure 12. Dynamic Quality Distribution. Non-homogeneous flow approach (Turner and Wallis [28]).

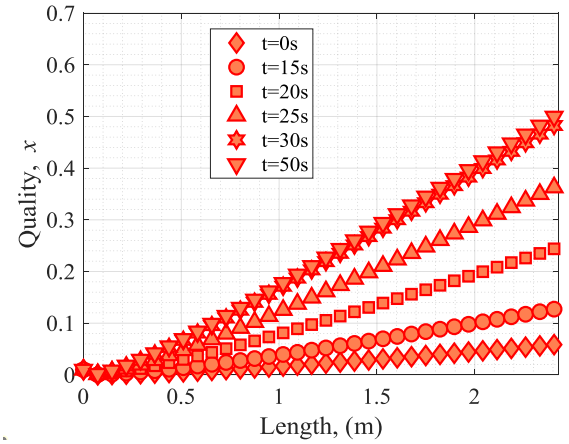

Fig. 13. Dynamic Quality Distribution. Non-homogeneous flow approach (Chen [33]).

Figures 12 and 13 show the dynamic quality distribution. The slip-ratio clearly affects the results, introducing a difference of 50% in the quality values obtained without slip. It is therefore important to validate the system under different slip-ratio models to enable a slip-ratio model recommendation. In this work, experiments will be performed and compared with results from existing correlations to obtain validated numerical and compact models.

Comparable results were found for heat transfer coefficient, wall temperature, local pressure and air temperature. In addition, the momentum equation; i.e., the local pressure distribution, is seem to have measurable effects on the quality distribution through the slip-ratio.

SUMMARY AND CONCLUSIONS

A computational model was developed for transient two phase flow and heat transfer applied to a cross-flow heat exchanger with air cooling on one side and refrigerant on the other. Through appropriate scaling, it was demonstrated that the energy and mass conservation equations for the refrigerant may be combined to form a single equation in refrigerant quality, which appears in nearly all the remaining equations

governing the system performance. It was shown that the energy equations for the wall and air stream may be reduced to a thermally lumped system, such that the temperatures depend only on time for both constituents.

From our results several comments are noteworthy.

1. It is observed that the gamma factor influences the local pressure prediction for the homogeneous and non-homogeneous flow approach. In the non-homogeneous method the advection term directly is affected through the function γ.
2. For the refrigerant equations, a slip-ratio upper and lower bound were investigated. This covers a wide range of possible solutions. Experimental validation is needed in order to provide a recommended slip-ratio correlation.
3. The lower bound adopted in this work is slightly more conservative compared with Awad and Muzychka [35]. They analyzed steady-state experimental data with void fraction models prediction and found that data is located between the limits proposed. Transient experimental data are needed to validate results such as void fraction or thermodynamic quality obtained with the numerical method.
4. Turner and Wallis slip-ratio predict higher vapor velocities compared with the velocity ratio predicted by Chen. The residence time for the gas phase is small, predicting low thermodynamic quality distribution.
5. The computational technique runs quickly. Challenges are observed related to the non-homogenous quality expression, where the derivative of the slip-ratio depending on the model chosen with respect to quality will become complicated according to the model chosen.
6. The local pressure variation is minor and can be assumed to be constant for purposes of thermodynamics calculations in the heat exchanger geometry considered. Moreover, cross-flow heat exchangers with smaller pipe diameters are used today. Hence, the pressure drop is significant on those heat exchangers and is the reason for considering the momentum equation.
7. The heat transfer coefficient in the refrigerant-side increase due to the temperature rising in the air inlet temperature into the heat exchanger. Therefore, the quality distribution predicted exhibits continuous growth in time and space as a result of the air temperature perturbation.

Future studies will include the upper and lower limits for the heat transfer coefficient and frictional pressure drop. Experimental measurements are underway in order to obtain data for model validation for a close-coupled cross-flow heat exchanger.

ACKNOWLEDGEMENTS

This material is based upon the work supported by the national Science Foundation Center for Energy Smart Electronic System (ES2) under the Grant No. IIP-1738782. Any opinions, findings, and conclusions or recommendations expressed in this material are those of the author(s) and do not necessarily reflect the views of the National Science Foundation.

References

[1] A. Capozzoli and G. Primiceri, "Cooling systems in data centers: state of art and emerging technologies," *Energy Procedia,* vol. 83, pp. 484-493, 2015.

[2] M. del Valle, C. Caceres, and A. Ortega, "Transient modeling and validation of chilled water based cross flow heat exchangers for local on-demand cooling in data centers," in *2016 15th IEEE Intersociety Conference on Thermal and Thermomechanical Phenomena in Electronic Systems (ITherm)*, 2016, pp. 727-736.

[3] M. del Valle and A. Ortega, "Numerical and compact models to predict the transient behavior of cross-flow heat exchangers in data center applications," in *Fourteenth Intersociety Conference on Thermal and Thermomechanical Phenomena in Electronic Systems (ITherm)*, 2014, pp. 698-705.

[4] M. del Valle and A. Ortega, "Experimental Characterization of the Transient Response of Air/Water Crossflow Heat Exchangers for Data Center Cooling Systems," in *ASME 2015 International Technical Conference and Exhibition on Packaging and Integration of Electronic and Photonic Microsystems collocated with the ASME 2015 13th International Conference on Nanochannels, Microchannels, and Minichannels*, 2015.

[5] M. Del Valle, C. Caceres, A. Ortega, K. Nemati, and B. Sammakia, "Quasi-steady modeling of data center heat exchanger under dynamic conditions," in *2017 16th IEEE Intersociety Conference on Thermal and Thermomechanical Phenomena in Electronic Systems (ITherm)*, 2017, pp. 878-884.

[6] T. Gao, J. Geer, and B. Sammakia, "Nonuniform temperature boundary condition effects on data center cross flow heat exchanger dynamic performance," *International Journal of Heat and Mass Transfer,* vol. 79, pp. 1048-1058, 2014.

[7] T. Gao, B. Sammakia, and J. Geer, "Dynamic response and control analysis of cross flow heat exchangers under variable temperature and flow rate conditions," *International Journal of Heat and Mass Transfer,* vol. 81, pp. 542-553, 2015.

[8] M. Willatzen, N. Pettit, and L. Ploug-Sørensen, "A general dynamic simulation model for evaporators and condensers in refrigeration. part i: moving-boundary formulation of two-phase flows with heat exchange: Modèle général dynamique pour évaporateurs et condenseurs frigorifiques. partic i: Formulation des conditions aux limites variables de flux biphasiques avec échange de chaleur," *International Journal of refrigeration,* vol. 21, pp. 398-403, 1998.

[9] B. D. Eldredge, B. P. Rasmussen, and A. G. Alleyne, "Moving-boundary heat exchanger models with variable outlet phase," *Journal of dynamic systems, measurement, and control,* vol. 130, 2008.

[10] E. W. Grald and J. W. MacArthur, "A moving-boundary formulation for modeling time-dependent two-phase flows," *International Journal of Heat and Fluid Flow,* vol. 13, pp. 266-272, 1992.

[11] X.-D. He, S. Liu, and H. H. Asada, "Modeling of vapor compression cycles for multivariable feedback control of HVAC systems," 1997.

[12] C.-C. Wang, "Recent progress on the air-side performance of fin-and-tube heat exchangers," *International Journal of Heat Exchangers,* vol. 1, pp. 49-76, 2000.

[13] M. Mishra, P. Das, and S. Sarangi, "Transient behavior of crossflow heat exchangers with longitudinal conduction and axial dispersion," *Journal of Heat Transfer,* vol. 126, pp. 425-433, 2004.

[14] M. Mishra, P. Das, and S. Sarangi, "Transient behaviour of crossflow heat exchangers due to perturbations in temperature and flow," *International journal of heat and mass transfer,* vol. 49, pp. 1083-1089, 2006.

[15] M. Mishra, P. Das, and S. Sarangi, "Effect of temperature and flow nonuniformity on transient behaviour of crossflow heat exchanger," *International Journal of Heat and Mass Transfer,* vol. 51, pp. 2583-2592, 2008.

[16] F. H. Syed and S. Idem, "Transient performance of a cross flow heat exchanger using finite difference analysis," in *ASME 2008 International Mechanical Engineering Congress and Exposition*, 2008, pp. 1333-1342.

[17] X. Jia, C. Tso, P. Chia, and P. Jolly, "A distributed model for prediction of the transient response of an evaporator," *International Journal of Refrigeration,* vol. 18, pp. 336-342, 1995.

[18] X. Jia, C. Tso, P. Jolly, and Y. Wong, "Distributed study of air temperature inside a dry-expansion evaporator," *Applied thermal engineering,* vol. 16, pp. 305-311, 1996.

[19] X. Jia, C. Tso, P. Jolly, and Y. Wong, "Distributed steady and dynamic modelling of dry-expansion evaporators: Modèlisation du régime stable et du régime transitoire des évaporateurs à détente sèche," *International Journal of Refrigeration,* vol. 22, pp. 126-136, 1999.

[20] R. Kapadia, S. Jain, and R. Agarwal, "Transient characteristics of split air-conditioning systems using R-22 and R-410A as refrigerants," *HVAC&R Research,* vol. 15, pp. 617-649, 2009.

[21] H. Müller-Steinhagen and K. Heck, "A simple friction pressure drop correlation for two-phase flow in pipes," *Chemical Engineering and Processing: Process Intensification,* vol. 20, pp. 297-308, 1986.

[22] X. Fang, Y. Xu, and Z. Zhou, "New correlations of single-phase friction factor for turbulent pipe flow and evaluation of existing single-phase friction factor correlations," *Nuclear Engineering and Design,* vol. 241, pp. 897-902, 2011.

[23] Z. Liu and R. Winterton, "A general correlation for saturated and subcooled flow boiling in tubes and annuli, based on a nucleate pool boiling equation," *International journal of heat and mass transfer,* vol. 34, pp. 2759-2766, 1991.

[24] M. G. Cooper, "Saturation Nucleat Boiling. A Simple Correlation," *1st U.K. Natn. Conf. on Heat Transfer,* vol. 2, pp. 285-793, 1984.

[25] H. S. Isbin, "One-dimensional two-phase flow, Graham B. Wallis, McGraw-Huill, New York (1969)," ed: Wiley Online Library, 1970.

[26] D. Chisholm, "Pressure gradients due to friction during the flow of evaporating two-phase mixtures in smooth tubes and channels," *International Journal of Heat and Mass Transfer,* vol. 16, pp. 347-358, 1973.

[27] C. Baroczy, "Correlation of liquid fraction in two-phase flow with application to liquid metals," Atomics International. Div. of North American Aviation, Inc., Canoga Park …1963.

[28] J. Turner and G. Wallis, "The separate-cylinders model of two-phase flow, paper no," *Paper No. NYO-3114-6, Thayer's School Engineering, Dartmouth College, Hanover, NH, USA,* 1965.

[29] S. Smith, "Void fractions in two-phase flow: a correlation based upon an equal velocity head model," *Proceedings of the Institution of Mechanical Engineers,* vol. 184, pp. 647-664, 1969.

[30] H. Nishino and Y. Yamazaki, "A new method of evaluating steam volume fractions in boiling systems," *Nippon Genshiryoku Gakkai-Shi,* vol. 5, 1963.

[31] R. Lockhart and R. Martinelli, "Proposed correlation of data for isothermal two-phase, two-component flow in pipes," *Chem. Eng. Prog,* vol. 45, pp. 39-48, 1949.

[32] P. Spedding and J. Chen, "Correlation and estimation of holdup in two-phase flow," in *Proc. NZ Geothermal Workshop*, 1979, pp. 180-199.

[33] J. Chen, "A further examination of void fraction in annular two-phase flow," *International Journal of Heat and Mass Transfer,* vol. 29, pp. 1760-1763, 1986.

[34] P. Hamersma and J. Hart, "A pressure drop correlation for gas/liquid pipe flow with a small liquid holdup," *Chemical engineering science,* vol. 42, pp. 1187-1196, 1987.

[35] M. Awad and Y. Muzychka, "Bounds on Two-Phase Flow: Part II—Void Fraction in Circular Pipes," in *ASME 2005 International Mechanical Engineering Congress and Exposition*, 2005, pp. 823-833.

[36] I. H. Bell, J. Wronski, S. Quoilin, and V. Lemort, "Pure and pseudo-pure fluid thermophysical property evaluation and the open-source thermophysical property library CoolProp," *Industrial & engineering chemistry research,* vol. 53, pp. 2498-2508, 2014.

Appendix

Wall Energy Equation Discretized

$$\Delta M_w c_w \left(\frac{T_{w_{i,j}}^{k+1} - T_{w_{i,j}}^{k}}{\Delta t}\right) + \Delta A_a \eta_f H_a (T_{w_{i,j}}^{k} - T_{a_{i,j}}^{k}) + \Delta A_r H_r (T_{w_{i,j}}^{k} - T_{r_{i,j}}^{k}) = 0 \quad \text{(A1)}$$

Air Energy Equation Discretized

$$\Delta M_a c_a \left(\frac{T_{a_{i,j}}^{k+1} - T_{a_{i,j}}^{k}}{\Delta t}\right) + \dot{m}_a c_a \left(T_{a_{i,j}}^{k+1} - T_{a_{i,j-1}}^{k+1}\right) + \Delta A_a \eta_f H_a (T_{a_{i,j}}^{k+1} - T_{w_{i,j}}^{k+1}) = 0 \quad \text{(A2)}$$

Homogeneous Energy Equation Distribution

$$\frac{\rho_v \rho_l h_{fg}}{\rho_v + x_i^{k+1}(\rho_l - \rho_v)} \left(\frac{x_i^{k+1} - x_i^{k}}{\Delta t}\right) + Gh_{fg} \left(\frac{x_i^{k+1} - x_{i-1}^{k+1}}{\Delta z}\right) + \frac{\pi D}{A_{c-a}} H_r (T_{r_i}^{k+1} - T_{w_i}^{k+1}) = 0 \quad \text{(A3)}$$

Refrigerant Momentum Equation

$$\frac{\left(\tilde{\rho} u\right)_i^{k+1} - \left(\tilde{\rho} u\right)_i^{k}}{\Delta t} + \frac{(\gamma \tilde{\rho} u^2)_i^{k+1} - (\gamma \tilde{\rho} u^2)_{i-1}^{k+1}}{\Delta z} = -\frac{p_i^{k+1} - p_{i-1}^{k+1}}{\Delta z} - f_z \quad \text{(A4)}$$

Non-Homogeneous Energy Equation Distribution (Turner and Wallis Upper Bound)

$$\frac{\rho_l h_{fg} \left(\left(\frac{\rho_l}{\rho_v} - 1\right) x_i^{k+1} + 1\right) \left(0.72 \left(\frac{x_i^{k+1}}{1 - x_i^{k+1}}\right)^{0.28} \left(\frac{\rho_l}{\rho_v}\right)^{0.6} \left(\frac{\mu_l}{\mu_v}\right)^{0.08}\right)}{\left(-\left(x_i^{k+1}\right)^{0.28} \left(1 - x_i^{k+1}\right)^{0.72} \left(\frac{\rho_l}{\rho_v}\right)^{0.6} \left(\frac{\mu_l}{\mu_v}\right)^{0.08} - \frac{\rho_l}{\rho_v} x_i^{k+1}\right)^2} \frac{x_i^{k+1} - x_i^{k+1}}{\Delta t} + Gh_{fg} \frac{x_i^{k+1} - x_{i-1}^{k+1}}{\Delta z} + \frac{\pi D}{A_{c-a}} H_r (T_{ri}^{k+1} - T_{wi}^{k+1}) = 0 \quad \text{(A5)}$$